Clim. Past, 10, 1211–1219, 2014
www.clim-past.net/10/1211/2014/
doi:10.5194/cp-10-1211-2014

Climate of the Past
Open Access

Stalagmite-inferred variability of the Asian summer monsoon during the penultimate glacial–interglacial period

T.-Y. Li[1,2,3], C.-C. Shen[3], L.-J. Huang[3], X.-Y. Jiang[4], X.-L. Yang[1], H.-S. Mii[5], S.-Y. Lee[6], and L. Lo[3]

[1]Key Laboratory of Eco-environments in Three Gorges Reservoir Region, Ministry of Education, School of Geographical Sciences, Southwest University, Chongqing 400715, China
[2]State Key Laboratory of Loess and Quaternary Geology, Institute of Earth Environment, CAS, Xi'an 710075, China
[3]High-Precision Mass Spectrometry and Environment Change Laboratory (HISPEC), Department of Geosciences, National Taiwan University, Taipei 10617, Taiwan, ROC
[4]College of Geographical Science, Fujian Normal University, Fuzhou 350007, China
[5]Department of Earth Sciences, National Taiwan Normal University, Taipei 11677, Taiwan, ROC
[6]Research Center for Environmental Changes, Academia Sinica, Taipei 11529, Taiwan, ROC

Correspondence to: C.-C. Shen (river@ntu.edu.tw)

Received: 29 October 2013 – Published in Clim. Past Discuss.: 11 November 2013
Revised: 25 April 2014 – Accepted: 25 April 2014 – Published: 24 June 2014

Abstract. The orbital-timescale dynamics of the Quaternary Asian summer monsoons (ASM) are frequently attributed to precession-dominated northern hemispheric summer insolation. However, this long-term continuous ASM variability is inferred primarily from oxygen isotope records of stalagmites, mainly from Sanbao cave in mainland China, and may not provide a comprehensive picture of ASM evolution. A new spliced stalagmite oxygen isotope record from Yangkou cave tracks summer monsoon precipitation variation from 124 to 206 thousand years ago in Chongqing, southwest China. Our Yangkou record supports that the evolution of ASM was dominated by the North Hemisphere solar insolation on orbital timescales. When superimposed on the Sanbao record, the precipitation time series referred from Yangkou cave stalagmites supports the strong ASM periods at marine isotope stages (MIS) 6.3, 6.5, and 7.1 and weak ASM intervals at MIS 6.2, 6.4, and 7.0. This consistency confirms that ASM events affected most of mainland China. Except for the solar insolation forcing, the large amplitude of minimum $\delta^{18}O$ values in Yangkou record during glacial period, such as MIS 6.5, could stem from the enhanced prevailing Pacific trade wind and/or continental shelf exposure in the Indo–Pacific warm pool.

1 Introduction

Climate in East Asia, the most densely populated region in the world, is profoundly influenced by the Asian monsoon (AM), which includes the Indian monsoon and East Asian monsoon sub-systems. Asian summer monsoon (ASM) precipitation strongly governs regional vegetation, agriculture, culture, and economies (e.g., Cheng et al., 2012a), and even affected the stability of Chinese dynastic rule (Zhang et al., 2008; Tan et al., 2011).

Our current understanding of ASM variation over the past 500 kyr BP (before AD 1950) has been reconstructed using oxygen isotope records of Chinese stalagmites (Wang et al., 2008; Cheng et al., 2012b) with the advantages of absolute and high-precision chronologies (e.g., Cheng et al., 2000, 2013; Shen et al., 2002, 2012). Stalagmite-inferred orbital-scale ASM intensity closely follows the change in precession-dominated northern hemispheric (NH) summer insolation (NHSI) (Wang et al., 2008; Cheng et al., 2012b). However, these 100s kyr records were mainly from a single cave, namely Sanbao cave, located in Hubei Province, China (Fig. 1; Wang et al., 2008; Cheng et al., 2012b). Utilizing only one site leads to uncertainties in the spatial extent of Quaternary ASM evolution. These uncertainties stem from differences in local or regional climatic and environmental conditions (Lachniet, 2009), hydrological variability

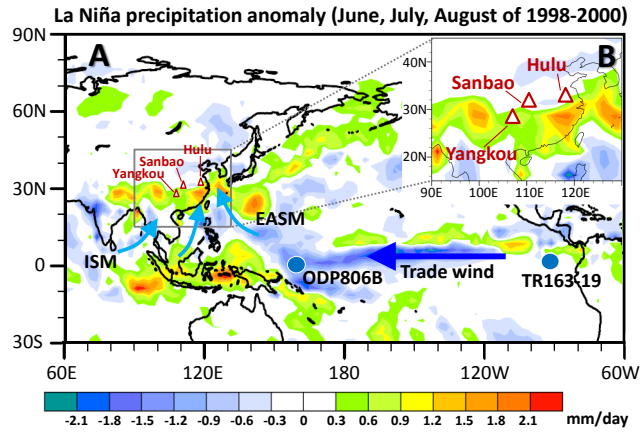

Figure 1. (A) Map of precipitation anomaly (mm day^{-1}) in June, July, and August (JJA) of AD 1998–2000 during a La Niña event from July 1998 to April 2001 (http://www.cpc.ncep.noaa.gov/products/analysis_monitoring/ensostuff/ensoyears.shtml) compared with the averaged state of JJA from 1980 to 2010. Triangle symbols denote cave sites of Yangkou (this study), Sanbao (Wang et al., 2008), and Hulu (Cheng et al., 2006). Solid circles indicate marine sediment cores of ODP806B and TR163-19 (Lea et al., 2000). Arrows depict present ground wind directions of the ISM and EASM and also trade wind in the equatorial Pacific. Summer precipitation intensity in eastern and southern China was enhanced during the La Niña event. **(B)** An enlarged map of precipitation anomaly with cave sites of Yangkou, Sanbao, and Hulu.

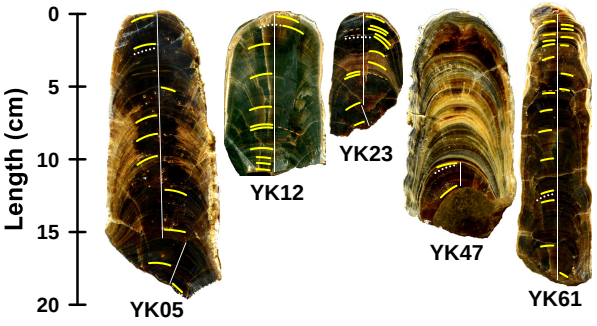

Figure 2. Photographs of the five stalagmites collected from Yangkou cave. Brown dashed curves show hiatuses. Straight lines represent subsampling routes for oxygen isotope measurement. Yellow curves denote drilled subsamples for U-Th dating. White dots are the subsamples collected for Hendy test (Hendy, 1971).

of monsoonal sources (e.g., Dayem et al., 2010; Clemens et al., 2010; Pausata et al., 2011), and interactions between climatic subsystems (e.g., Maher and Thompson, 2012; Tan, 2014).

Sanbao records, for example, show distinct ASM events at marine isotope stages (MIS) 6.3 and 6.5 during the penultimate glacial time and a weaker summer monsoon during the penultimate glacial maximum (PGM) at MIS 6.2 (Fig. 1 of Wang et al., 2008). To clarify whether this combination of weak PGM ASM intensities and strong ASM events during the penultimate glacial–interglacial (G–IG) period are local effects, we built an integrated stalagmite oxygen stable isotope record from Yangkou cave, Chongqing, China, covering 124–206 kyr BP (Fig. 1). Through comparison with records from other Chinese caves (Cheng et al., 2006, 2009; Wang et al., 2008) confirms the fidelity of Sanbao cave-inferred ASM intensities.

2 Material and methods

2.1 Regional settings and samples

Stalagmites were collected from Yangkou cave (29°02′ N, 107°11′ E; altitude: 2140 m; length: 2245 m), located at Jinfo Mountain National Park, Chongqing City, southwestern China (Fig. 1) during two field trips in October 2010 and July 2011. The cave, developed in Permian limestone bedrock, is 400 km southwest of Sanbao cave (31°40′ N, 110°26′ E) in Hubei Province (Wang et al., 2008). The cave air temperature is 7.5 °C and the average relative humidity is > 80 % (October 2011–October 2013). The regional climate is influenced by both the Indian summer monsoon (ISM) and East Asian summer monsoon (EASM). Annual rainfall is 1400–1500 mm, 83 % from April to October (Zhang et al., 1998). Five stalagmites, YK05, YK12, YK23, YK47, and YK61, which formed within a time interval of 124–206 kyr BP, were halved and polished for U-Th dating and oxygen stable isotope analysis.

2.2 U-Th dating

Chemistry and instrumental analysis were conducted in the High-Precision Mass Spectrometry and Environment Change Laboratory (HISPEC), Department of Geosciences, National Taiwan University. Fifty three powdered subsamples, 60–80 mg each, were drilled from the polished surface along the deposit lamina of the five stalagmites (Fig. 2, Table 1), on a class-100 bench in a class-10 000 subsampling room. U-Th chemistry (Shen et al., 2003) was performed in a class-10 000 clean room with independent class-100 benches and hoods (Shen et al., 2008). A multi-collector inductively coupled plasma mass spectrometer (MC-ICP-MS), Thermo Fisher Neptune with secondary electron multiplier protocols was used for the determination of U-Th isotopic contents and compositions (Shen et al., 2012). The decay constants used are 9.1577×10^{-6} yr^{-1} for ^{230}Th, 2.8263×10^{-6} yr^{-1} for ^{234}U (Cheng et al., 2000), and 1.55125×10^{-10} yr^{-1} for ^{238}U (Jaffey et al., 1971). All errors of U-Th isotopic data and U-Th dates are two standard deviations (2σ) unless otherwise noted. Age (before AD 1950) corrections were made using an ^{230}Th / ^{232}Th atomic ratio of 4 ± 2 ppm, which are the values for material at secular equilibrium with the crustal ^{232}Th / ^{238}U value of 3.8 (Taylor and McLennan, 1995) and an arbitrary uncertainty of 50 %.

Table 1. U-Th isotopic compositions and ^{230}Th ages for subsamples of five Yangkou stalagmites on MC-ICP-MS at the HISPEC, NTU.

	Subsample ID	Depth (mm)	^{238}U (ppb)	^{232}Th (ppt)	δ^{234}U measured[a]	[^{230}Th / ^{238}U] activity[c]	[^{230}Th / ^{232}Th] (ppm)[d]	Age (kyr) uncorrected	Age (kyr, BP) corrected[c,e]	δ^{234}Uinitial corrected[b]
Stalagmite: YK5	YK5-01	3.0	8730 ± 13	553.0 ± 7.1	215.8 ± 2.1	1.0192 ± 0.0024	265 626 ± 3445	179.7 ± 1.3	179.6 ± 1.3	358.5 ± 3.7
	YK5-02	24.0	7335 ± 14	263.1 ± 7.1	218.4 ± 2.7	1.0235 ± 0.0027	471 128 ± 12 563	180.4 ± 1.6	180.4 ± 1.6	363.6 ± 4.8
	YK5-03	57.0	4322.4 ± 7.6	5997 ± 17	192.9 ± 2.3	1.0002 ± 0.0024	11 903 ± 39	181.2 ± 1.4	181.1 ± 1.4	321.9 ± 4.1
	YK5-04	79.0	5041 ± 10	500.2 ± 5.7	187.7 ± 2.9	0.9997 ± 0.0026	166 348 ± 1928	183.2 ± 1.7	183.2 ± 1.7	315.1 ± 5.0
	YK5-05	88.0	5729.6 ± 9.4	356.1 ± 5.1	184.6 ± 2.4	0.9986 ± 0.0027	265 267 ± 3814	184.2 ± 1.6	184.1 ± 1.6	310.6 ± 4.2
	YK5-06	103.0	5375.3 ± 9.9	593.2 ± 5.0	202.1 ± 2.6	1.0161 ± 0.0022	152 028 ± 1290	184.2 ± 1.5	184.1 ± 1.5	340.1 ± 4.7
	YK5-07	128.0	4986.2 ± 8.8	137.6 ± 5.8	201.6 ± 2.3	1.0175 ± 0.0023	608 876 ± 25 827	185.1 ± 1.4	185.0 ± 1.4	340.0 ± 4.1
	YK5-08	149.0	6076 ± 14	269.0 ± 5.2	205.0 ± 3.0	1.0259 ± 0.0028	382 639 ± 7471	187.2 ± 1.8	187.2 ± 1.8	348.1 ± 5.3
	YK5-09	177.0	8808 ± 11	1103.7 ± 7.2	215.0 ± 1.9	1.0374 ± 0.0016	136 699 ± 889	187.9 ± 1.1	187.8 ± 1.1	365.7 ± 3.5
	YK5-10	188.0	12 100 ± 19	168.3 ± 6.1	210.0 ± 2.5	1.0368 ± 0.0027	1 230 671 ± 44 610	189.9 ± 1.7	189.8 ± 1.7	359.2 ± 4.7
Stalagmite: YK12	YK12-01	3.6	6262.6 ± 4.1	3895 ± 24	309.6 ± 1.2	0.9620 ± 0.0015	25 540 ± 164	133.76 ± 0.46	133.69 ± 0.46	451.8 ± 1.9
	YK12-02	10.5	5016.7 ± 2.5	12 393 ± 25	296.1 ± 1.2	0.9590 ± 0.0017	6410 ± 17	135.88 ± 0.51	135.78 ± 0.51	434.7 ± 1.8
	YK12-03	21.5	6384.1 ± 3.6	1050 ± 21	296.2 ± 1.1	0.9796 ± 0.0014	98 334 ± 1947	141.43 ± 0.46	141.36 ± 0.46	441.8 ± 1.7
	YK12-04	40.0	5675.3 ± 5.8	9675 ± 32	273.0 ± 1.6	0.9792 ± 0.0017	9483 ± 34	147.07 ± 0.67	146.98 ± 0.67	413.7 ± 2.6
	YK12-05	57.5	13 314 ± 13	1488 ± 21	259.4 ± 1.5	0.9840 ± 0.0015	145 382 ± 2094	152.20 ± 0.62	152.14 ± 0.62	398.9 ± 2.4
	YK12-06	78.0	1746.6 ± 5.5	1425 ± 24	253.54 ± 0.90	0.9852 ± 0.0013	134 061 ± 2272	154.30 ± 0.49	154.24 ± 0.49	392.1 ± 1.5
	YK12-07	80.0	8830.3 ± 5.3	38 573 ± 98	212.8 ± 1.2	0.9796 ± 0.0027	3702 ± 14	165.3 ± 1.1	165.1 ± 1.1	339.4 ± 2.2
	YK12-08	92.0	7106.6 ± 3.6	7546 ± 25	199.70 ± 0.89	0.9823 ± 0.0014	15 274 ± 55	171.08 ± 0.64	170.99 ± 0.64	323.9 ± 1.5
	YK12-09	101.0	9513.1 ± 6.5	4483 ± 23	203.4 ± 1.1	0.9976 ± 0.0013	34 954 ± 182	175.80 ± 0.72	175.73 ± 0.72	334.3 ± 2.0
	YK12-10	105.0	5118.6 ± 6.7	2378 ± 21	185.4 ± 1.9	0.9924 ± 0.0018	35 265 ± 317	181.0 ± 1.1	180.9 ± 1.1	309.3 ± 3.3
	YK12-11	109.5	6109.1 ± 3.8	572 ± 18	178.4 ± 1.2	0.9875 ± 0.0013	174 125 ± 5633	181.93 ± 0.77	181.87 ± 0.77	298.4 ± 2.1
Stalagmite: YK23	YK23-01	2.4	2893.2 ± 2.3	13 899 ± 26	102.8 ± 1.5	0.8935 ± 0.0018	3070.9 ± 8.0	172.8 ± 1.0	172.6 ± 1.0	167.6 ± 2.4
	YK23-02	9.6	2608.9 ± 1.7	13 210 ± 23	99.6 ± 1.1	0.9008 ± 0.0016	2937.3 ± 7.1	177.70 ± 0.95	177.53 ± 0.95	164.5 ± 1.9
		Hiatus								
	YK23-03	11.2	2705.2 ± 1.3	1370 ± 17	59.55 ± 0.91	0.8799 ± 0.0016	28 683 ± 355	187.3 ± 1.0	187.3 ± 1.0	101.1 ± 1.6
	YK23-04	14.8	2541.1 ± 1.2	10 313 ± 20	60.06 ± 0.89	0.8830 ± 0.0015	3592.3 ± 8.9	188.73 ± 0.98	188.57 ± 0.98	102.4 ± 1.5
		Hiatus								
	YK23-05	16.8	3255.5 ± 2.0	1365 ± 14	32.5 ± 1.1	0.8632 ± 0.0012	33 986 ± 363	193.47 ± 0.99	193.40 ± 0.99	56.1 ± 1.8
	YK23-06	27.6	3084.7 ± 1.5	2354 ± 14	32.53 ± 0.92	0.8671 ± 0.0012	18 764 ± 112	195.87 ± 0.93	195.79 ± 0.93	56.6 ± 1.6
	YK23-07	35.6	2208.7 ± 1.3	2343 ± 15	47.1 ± 1.0	0.8848 ± 0.0014	13 768 ± 89	197.5 ± 1.1	197.5 ± 1.1	82.2 ± 1.8
	YK23-08	42.4	1917.04 ± 0.90	4503 ± 17	39.3 ± 1.1	0.8795 ± 0.0013	6182 ± 25	199.3 ± 1.1	199.2 ± 1.1	68.9 ± 1.9
		Hiatus								
	YK23-09	43.0	2720.4 ± 1.5	1128 ± 14	21.23 ± 0.90	0.8633 ± 0.0013	34 369 ± 430	201.0 ± 1.1	200.9 ± 1.1	37.5 ± 1.7
	YK23-10	62.4	3355.3 ± 2.2	698 ± 23	16.2 ± 1.0	0.8657 ± 0.0014	68 753 ± 2263	206.2 ± 1.2	206.1 ± 1.2	29.0 ± 1.8
	YK23-11	77.2	2262.6 ± 1.5	899 ± 19	15.0 ± 1.1	0.8655 ± 0.0015	35 976 ± 777	206.9 ± 1.3	206.8 ± 1.3	26.9 ± 2.1
Stalagmite: YK47	YK47-01	118.8	812.37 ± 0.81	6437 ± 11	395.2 ± 1.8	1.0173 ± 0.0022	2120.0 ± 6.0	130.19 ± 0.61	129.99 ± 0.61	570.7 ± 2.8
	YK47-02	137.5	765.96 ± 0.70	2997.5 ± 7.6	398.9 ± 1.8	1.0295 ± 0.0019	4343 ± 13	132.27 ± 0.57	132.14 ± 0.57	579.7 ± 2.8
Stalagmite: YK61	YK61-01	13.6	3427.4 ± 2.1	13 736 ± 25	295.8 ± 1.2	0.9172 ± 0.0019	3779 ± 10	125.39 ± 0.51	125.26 ± 0.51	421.5 ± 1.8
	YK61-02	15.5	3636.8 ± 1.9	4502 ± 12	275.4 ± 1.2	0.9027 ± 0.0013	12 039 ± 37	125.80 ± 0.41	125.72 ± 0.41	393.0 ± 1.8
	YK61-03	17.0	3974.8 ± 2.4	4663 ± 10	261.5 ± 1.2	0.8936 ± 0.0013	12 577 ± 32	126.29 ± 0.41	126.21 ± 0.41	373.6 ± 1.8
	YK61-04	20.0	3418.6 ± 3.7	1271.0 ± 8.9	302.6 ± 1.8	0.9278 ± 0.0013	41 205 ± 291	126.64 ± 0.48	126.58 ± 0.48	432.9 ± 2.6
	YK61-05	22.4	1520.4 ± 2.4	3627 ± 33	340.2 ± 2.4	0.9619 ± 0.0024	6658 ± 63	127.60 ± 0.72	127.50 ± 0.72	487.8 ± 3.5
	YK61-06	26.0	2414.5 ± 4.3	2217 ± 29	315.2 ± 2.4	0.9448 ± 0.0027	16 993 ± 229	128.33 ± 0.80	128.25 ± 0.80	453.0 ± 3.6
	YK61-07	28.3	4454.4 ± 4.8	801.0 ± 8.8	313.7 ± 1.7	0.9452 ± 0.0013	86 784 ± 959	128.70 ± 0.47	128.63 ± 0.47	451.4 ± 2.5
	YK61-08	30.1	2434.4 ± 2.3	657.4 ± 8.6	314.5 ± 1.6	0.9479 ± 0.0012	57 958 ± 756	129.21 ± 0.43	129.15 ± 0.43	453.1 ± 2.3
	YK61-09	40.8	3633.5 ± 4.6	207 ± 25	302.5 ± 2.1	0.9389 ± 0.0019	271 567 ± 32 442	129.37 ± 0.64	129.31 ± 0.64	436.1 ± 3.2
	YK61-10	47.8	3140.5 ± 3.0	132.3 ± 7.0	305.6 ± 1.6	0.9459 ± 0.0013	370 865 ± 19 563	130.52 ± 0.45	130.46 ± 0.45	441.9 ± 2.3
	YK61-11	61.3	5420.5 ± 6.6	3648 ± 10	306.2 ± 1.8	0.9502 ± 0.0016	23 311 ± 67	131.47 ± 0.55	131.39 ± 0.55	443.9 ± 2.7
		Hiatus								
	YK61-12	63.1	2307.3 ± 1.8	1947.5 ± 8.3	303.9 ± 1.3	0.9801 ± 0.0012	19 171 ± 84	139.78 ± 0.45	139.70 ± 0.45	451.0 ± 2.0
	YK61-13	74.0	5853.2 ± 7.4	3435 ± 11	287.2 ± 1.7	0.9743 ± 0.0017	27 409 ± 90	142.09 ± 0.63	142.01 ± 0.63	429.2 ± 2.7
	YK61-14	88.0	3614.8 ± 7.1	352 ± 20	321.2 ± 2.9	1.0365 ± 0.0027	175 586 ± 9727	151.4 ± 1.1	151.3 ± 1.1	492.7 ± 4.7
	YK61-15	110.0	4705.3 ± 8.5	672 ± 16	320.3 ± 2.6	1.0476 ± 0.0026	121 199 ± 2976	154.9 ± 1.1	154.9 ± 1.1	496.2 ± 4.4
	YK61-16	130.0	5173.2 ± 8.0	646 ± 18	303.7 ± 2.3	1.0495 ± 0.0022	138 661 ± 3763	160.25 ± 0.98	160.18 ± 0.98	477.6 ± 3.8
	YK61-17	137.8	6174.8 ± 8.5	405.3 ± 7.9	299.4 ± 2.0	1.0514 ± 0.0019	264 459 ± 5140	162.16 ± 0.87	162.10 ± 0.87	473.5 ± 3.4
	YK61-18	167.8	4766.3 ± 5.3	347.8 ± 7.3	274.1 ± 1.7	1.0478 ± 0.0014	237 115 ± 4998	169.06 ± 0.77	168.99 ± 0.77	441.9 ± 3.0
	YK61-19	185.8	2984.1 ± 2.9	1897.4 ± 9.4	239.0 ± 1.7	1.0238 ± 0.0015	26 585 ± 135	172.56 ± 0.84	172.49 ± 0.84	389.2 ± 2.9

Chemistry was performed during 2011–2012 (Shen et al., 2003) and instrumental analyses on MC-ICP-MS (Shen et al., 2012). Analytical errors are 2σ of the mean.

[a] $\delta^{234}\mathrm{U} = ([^{234}\mathrm{U}/^{238}\mathrm{U}]_{\mathrm{activity}} - 1) \cdot 1000$.

[b] δ^{234}U initial corrected was calculated based on ^{230}Th age (T), i.e., $\delta^{234}\mathrm{U}_{\mathrm{initial}} = \delta^{234}\mathrm{U} \cdot e^{\lambda 234 \cdot T}$, and T is corrected age.

[c] $[^{230}\mathrm{Th}/^{238}\mathrm{U}]_{\mathrm{activity}} = 1 - e^{-\lambda 230 T} + (\delta^{234}\mathrm{U}/1000)[\lambda_{230}/(\lambda_{230} - \lambda_{234})](1 - e^{-(\lambda 230 - \lambda 234)T})$, where T is the age.
Decay constants used are available in Cheng et al. (2000).

[d] The degree of detrital ^{230}Th contamination is indicated by the [^{230}Th/^{232}Th] atomic ratio instead of the activity ratio.

[e] Age [yr BP (before AD 1950)] corrections were made using an ^{230}Th/^{232}Th atomic ratio of 4 ± 2 ppm.
Those are the values for material at secular equilibrium, with the crustal ^{232}Th/^{238}U value of 3.8. The errors are arbitrarily assumed to be 50 %.

2.3 Stable isotopes

Five-to-seven coeval subsamples, 60–120 µg each, were drilled from one layer per stalagmite to measure the oxygen and carbon isotopic compositions as part of the so-called "Hendy test" (Hendy, 1971). To obtain oxygen time series, 604 subsamples, 60–120 µg each, were drilled at 0.5–3.0 mm intervals along the maximum growth axis. Measurement of oxygen stable isotopes was performed by two isotope ratio mass spectrometers, including a Finnigan Delta V Plus in the Southwest University, China, and a Micromass IsoPrime instrument at the National Taiwan Normal University. Oxygen isotope values were reported as δ^{18}O (‰) with respect to the Vienna Pee Dee Belemnite standard (V-PDB). An international standard, NBS-19, was used in both laboratories to confirm that the 1σ standard deviation of δ^{18}O was better than ± 0.1 ‰.

3 Results and discussion

3.1 Chronology

U-Th isotopic and concentration data and dates of all stalagmite subsamples are given in Table 1. High uranium levels range from 0.8 to 13 ppm and relatively low thorium contents from 100 s to 10 000 ppt. Corrections for initial ^{230}Th are less than 90 years, much smaller than dating uncertainties of 400–1800 years that are common for stalagmites with these ^{230}Th ages (Table 1). Determined age intervals are 179.6–189.8, 133.7–181.9, 172.6–206.8, 130.0–132.1, and 97.2–172.5 kyr BP for stalagmites YK05, YK12, YK23, YK47, and YK61, respectively (Fig. 3). One to two hiatuses are observed for stalagmites YK12, YK23, and YK61 (Figs. 2, 3). The chronology of each stalagmite was developed using linear interpolation between U-Th dates, which are all in stratigraphic order (Fig. 3).

3.2 Yangkou oxygen isotope data

The well-known Hendy test has been taken as an essential requirement when assessing the ability of stalagmites to serve as paleoclimate archives (Hendy, 1971) (Fig. 4). Despite relative large δ^{13}C variations of 0.1–0.4 ‰ (1σ) for coeval subsamples on the five selected layers (Fig. 4a), only a small variations in δ^{18}O of $\pm 0.1 - 0.2$ ‰ (1σ) are observed on individual horizons of coeval subsamples (Fig. 4b). There is no relationship ($0.01 < r^2 < 0.36$) between δ^{18}O and δ^{13}C values for coeval subsamples of four layers (Fig. 4c), which is an additional part of the Hendy test. Although an apparent high correlation ($r^2 = 0.94$) for the plot of δ^{18}O versus δ^{13}C is expressed for the depth of 134.3 mm of stalagmite YK61 (Fig. 4c), the δ^{18}O values, from -8.2 ‰ to -8.4 ‰, change only 0.2 ‰. The absence of a clear increasing δ^{18}O trend outward on the same layer (Fig. 4b) also suggests an insignificant effect of kinetic fractionation. The replication of the

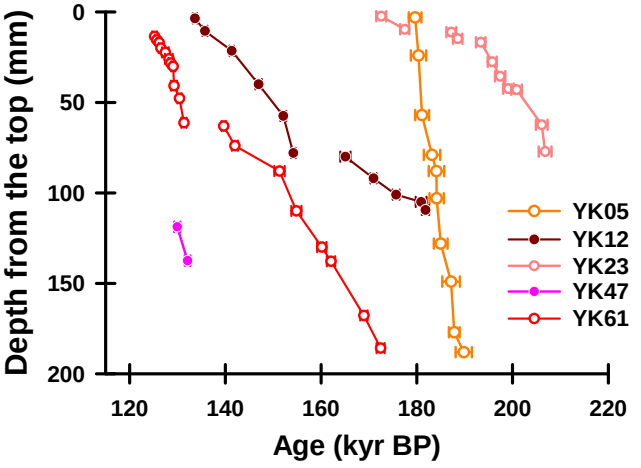

Figure 3. Age models of Yangkou stalagmites, established with U-Th dates with 2σ precisions of $\pm 0.3 - 1.0$ % (horizontal error bars).

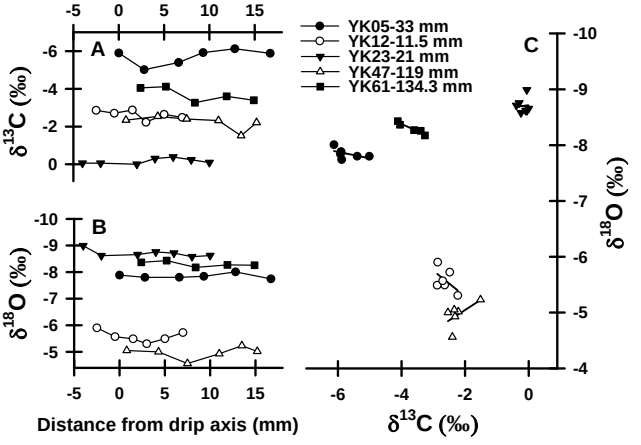

Figure 4. Hendy test on the arbitrarily selected laminae of five stalagmites with coeval data of **(A)** δ^{13}C and **(B)** δ^{18}O. **(C)** Plots of δ^{18}O versus δ^{13}C for coeval subsamples.

δ^{18}O records both within Yangkou cave (Fig. 5) and between Chinese caves (Fig. 6), as well as successful Hendy tests, indicates that the stalagmites formed under an oxygen isotopic equilibrium condition. The Yangkou stalagmite δ^{18}O data therefore represent rainfall oxygen isotopic change, which is a reflection of regional hydrological variability in the AM territory (e.g., Wang et al., 2001, 2008; Cheng et al., 2009; Li et al., 2011).

The oxygen isotope sequences for all of the Yangkou stalagmites are illustrated in Fig. 5a. The spliced record covers a time interval from 124 to 206 kyr BP, with three narrow hiatuses at 132.1–133.5, 190.4–193.2, and 200.3–200.9 kyr BP. This δ^{18}O record varies from -10 ‰ to -4 ‰. The highest δ^{18}O data of -5 ‰ ~-4 ‰ occurs at 128–136 kyr BP, the PGM.

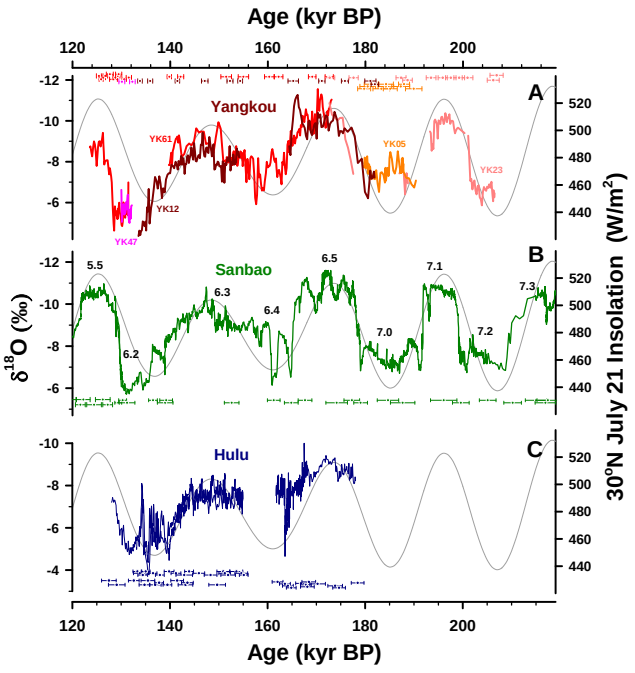

Figure 5. Cave stalagmite oxygen isotope records of **(A)** Yangkou (this study), **(B)** Sanbao (Wang et al., 2008; Cheng et al., 2009), and **(C)** Hulu (Cheng et al., 2006). U-Th ages and 2σ errors were color-coded by stalagmite. Numbers of MIS 5.5–7.3 are given by Sanbao record. Gray line is NHSI on 21 July at 30° N.

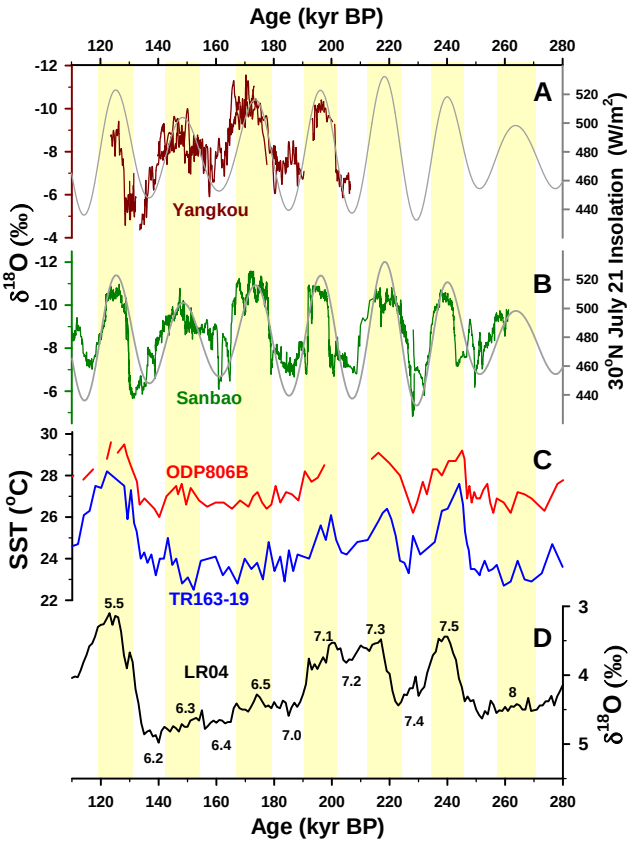

Figure 6. Comparison of Chinese cave δ^{18}O records of **(A)** Yangkou and **(B)** Sanbao (Wang et al., 2008; Cheng et al., 2009) with **(C)** reconstructed SST records in the WPWP (core ODP806B) and EEP (core TR163-19) (Lea et al., 2000), and **(D)** a global stack benthic foraminifer δ^{18}O sequence LR04 (Lisiecki and Raymo, 2005). Numbers of MIS 5.5–8 are given by LR04 record. Gray line is NHSI on 21 July at 30° N. Vertical bars denote high insolation intervals.

3.3 Comparison with other Chinese stalagmite records

The new spliced stalagmite δ^{18}O sequence from Yangkou cave over the time period of 124–206 kyr BP shows four strong ASM intervals at MIS 5.5, 6.3, 6.5, and 7.1 and four weak ASM intervals corresponding to MIS 6.2, MIS 6.4, MIS 7.0, and MIS 7.2 (Fig. 5a). This variation of stalagmite-inferred ASM recorded in Yangkou cave is aligned with previous ASM changes from other Chinese caves, such as Sanbao (Wang et al., 2008; Cheng et al., 2009) and Hulu (32°30′ N, 119°10′ E) (Cheng et al., 2006), from MIS 5.5 to 7.2 (Fig. 5).

The onsets of strong ASM intervals at MIS 5.5, 6.5, and 7.1 are at 128.3 ± 0.8, 179.9 ± 0.9, and 201.5 ± 1.1 kyr BP, respectively, in the Yangkou record and concurrent with their counterparts in Sanbao (Wang et al., 2008; Cheng et al., 2009) and Hulu (Cheng et al., 2006). Transients from strong to weak ASM states occur at 135–136 kyr BP during MIS 6.2–6.3, and 164–165 kyr BP during MIS 6.4–6.5. These also match changes in the Sanbao and Hulu records.

Over the past 200 kyr BP, the weakest ASM interval has been suggested to be at MIS 6.2 in the Sanbao records (Wang et al., 2008). For example, the δ^{18}O data are 1 ‰ higher than those at weak ASM intervals of MIS 6.4, 7.0, and 7.2 (Fig. 5). Concurrence between ASM records and ice-rafted debris events in the North Atlantic supports the hypothesis of a NH high-latitude forcing of the ASM (Cheng et al., 2009). δ^{18}O values at MIS 6.2 in Yangkou record are 1.5–2 ‰ higher than those at MIS 6.4, 7.0, and 7.2 (Fig. 5). This large difference suggests that this event in Chongqing may have been relatively intensified through NH forcing as compared with the Hubei regions during the PGM.

The Sanbao record indicates that the strongest ASM condition over the past 500 kyr BP occurs at MIS 6.5 (Cheng et al., 2012b). This ASM event, lasting 13 kyr, is 3 kyr longer than a comparable event (in terms of intensity) at interglacial MIS 5.3, and was stronger than at any time during MIS 1, 5.5, 7.3, 9.5, and 11.3, which experienced higher sea level and NH insolation (Fig. 1 of Cheng et al., 2012b). The lowest contemporaneous δ^{18}O data in the Yangkou record (Fig. 5) show a similar ASM intensity at MIS 6.5 in southwest China.

During the MIS 5, the variations of Chinese stalagmite δ^{18}O records are not consistent among caves (Cheng et al., 2012). In Sanbao record (Wang et al., 2008), the δ^{18}O

minimum at MIS 5.3 is more depleted than at MIS 5.5. This phenomenon is seemingly illustrated in Yangkou records (Fig. 5a). However, Dongge (Kelly et al., 2006) and Tianmen (Cai et al., 2010a) stalagmite records are characterized by the most depletion in ^{18}O at MIS 5.5 (Fig. 2 of Cai et al., 2010a). This discrepancy may be attributable to different hydrological conditions at MIS 5. Long time series from more Chinese caves are required to derive a clear picture of amplitude changes in relation to orbital forcing at MIS 5.

Overall, consistency of the stalagmite $\delta^{18}O$ sequences between Yangkou and other Chinese caves supports the idea that ASM intensity primarily follows NHSI on orbital timescales and is driven by precessional forcing and is punctuated by NH high-latitude climatic fluctuations (e.g., Wang et al., 2001, 2008; Cheng et al., 2009). Agreement in the amplitude and the transition of $\delta^{18}O$ dynamics during different MIS also confirms that the Sanbao stalagmite-inferred ASM events at MIS 6, including a very weak one at MIS 6.2 and the strongest one at MIS 6.5, are likely predominant over the entire mainland during the penultimate G–IG cycles (Cheng et al., 2012a) (Fig. 6).

3.4 Forcings for the abnormally strong ASM at MIS 6.5

The extraordinarily strong ASM condition at MIS 6.5 during the penultimate glacial period is one of the most striking features revealed by stalagmite records from three different Chinese caves (Fig. 5). This strong summer monsoon event is also observed in Chinese Loess plateau record (Rousseau et al., 2009). Modeling experiments suggest this increased monsoon intensity is primarily attributed to high NH insolation (Masson et al., 2000).

Wang et al. (2008) found a correlation between the stalagmite-inferred ASM intensity and the atmospheric $\delta^{18}O$ records from Antarctic Vostok ice-core O_2 bubbles (Sowers et al., 1991; Petit et al., 1999), and suggested that the Dole effect (Dole, 1936; Bender et al., 1994) can explain this similarity. A minimum atmospheric $\delta^{18}O$ ($\delta^{18}O_{atm}$) peak at 170 kyr BP in the Vostok ice core (Petit et al., 1999), for example, matches the strong-ASM period at MIS 6.5.

The evolution of $\delta^{18}O_{atm}$ inferred from the Vostok ice core most likely results from changes in summer insolation and precipitation in NH, where land provides space for the growth of vegetation and photosynthesis during glacial periods (Sun et al., 2000). However, the summer insolation at MIS 6.5 is less than the interglacial periods at MIS 5.5 and 7.3 (Fig. 5), suggesting that the minimal stalagmite $\delta^{18}O$ values at MIS 6.5 could also be associated with additional secondary forcing(s).

Climate conditions around Yangkou and Sanbao caves are influenced by the Indian summer monsoon (ISM) and East Asian summer monsoon (EASM) (Fig. 1). The ISM is primarily driven by a south–north land–sea thermal gradient; instead, the EASM is controlled by both south–north and east–west land–sea gradients (Wang and Lin, 2002). The EASM precipitation is influenced by the northwestern Pacific tropical high, developed by the mainland-Pacific thermal gradient (Wang et al., 2003). The Pacific climatic variability can, therefore, affect EASM precipitation (Tan, 2014).

Cai et al. (2010b) and Jiang et al. (2012) argued for a significant impact of the western tropical Pacific sea surface temperature (SST) on the EASM precipitation. They proposed that the evolution and spatial asynchroneity of stalagmite-inferred Holocene precipitation histories at different AM regions could be attributed to SST changes in the western Pacific. Planktonic foraminiferal-inferred SST records of the marine sediment core ODP806B (0°19′ N, 159°22′ E) in the western Pacific warm pool (WPWP) and TR163-19 (2°16′ N, 90°57′ W) in the eastern equatorial Pacific (EEP) (Lea et al., 2000) are plotted in Fig. 6, along with the LR04 stacked benthic $\delta^{18}O$ sequence (Lisiecki and Raymo, 2005) and Yangkou and Sanbao cave time series. A SST gradient between the WPWP and EEP during the glacial periods of MIS 6 and 8 is 2 °C, larger than the 0.5–1.5 °C gradient during the warm interglacial windows of MIS 5.5 and 7 (Fig. 6). Combined with salinity gradient data, Lea et al. (2000) suggested that the transport of water vapor to the western Pacific was enhanced during glacial times. This large SST gradient could result in an enhanced Walker circulation in the Pacific, similar to the modern La Niña state, which moves the rainfall zone westward and intensifies EASM precipitation (Clement et al., 1999) (Fig. 1). Under a weak Walker circulation, analogous to present El Niño conditions, the rainfall zone in the Pacific migrated eastward and EASM precipitation was reduced (Clement et al., 1999). We speculate that the extremely strong EASM precipitation at MIS 6.5 was not only governed by high NHSI, but also partially affected by the Pacific SST gradient.

This speculation is supported by modern meteorological observations (e.g., Xue et al., 2007; Tan, 2014) and resolved decadal marine records (Oppo et al., 2009). La Niña years accompany precipitation probabilities above normal in mainland China (Tan, 2014, and references therein). However, comparison of SST histories in the South China Sea and eastern equatorial Pacific SST suggests an El Niño-like condition for the last glacial time (Koutavas et al., 2002), opposite to the findings by Lea et al. (2000). The study by Koutavas et al. (2002) does not support our argument at MIS 6.5.

Sea level change could be one of the secondary factors. Marine proxy records and model simulations show that the exposure of the Sunda shelf at the Last Glacial Maximum (LGM) associated with a low sea level condition can alters regional hydrologic pattern in Southeast Asia (DiNezio and Tierney, 2013). During the LGM, the strong Pacific equatorial SST gradient could strengthen the Pacific Walker circulation and increase rainfall in the west tropical Pacific. As pointed out by DiNezio and Tierney (2013), both of the proxies and model simulations are highly uncertain renditions of climate history, and thus multi-proxy records and high precise models are critical to understand paleoclimate.

3.5 Abrupt ASM changes

One prominent feature of ASM dynamics is the occurrence of sudden δ^{18}O shifts at about the midpoint of precession-dominated NHSI change expressed in all Chinese caves over the study time window (Kelly et al., 2006; Cai et al., 2010a; Wang et al., 2008; Cheng et al., 2012a) (Fig. 5). For example, the jumps from weak to strong ASM states lasted < 100 years from MIS 6.2 to 5.5 and 500 years from MIS 7.2 to 7.1 (this study; Wang et al., 2008; Cheng et al., 2009). Climate in Hulu Cave is primarily dominated by EASM; on the other hand, Yangkou and Sanbao caves are located in a region influenced by both EASM and ISM. This agreement of local abrupt δ^{18}O changes supports the synchroneity of both monsoon sub-system variations on precessional timescale (e.g., Cheng et al., 2012a) and confirms the robustness and regionality of these abrupt transitions in the vast ASM territory. Yangkou records also support the phase lag between ASM and NHSI (Cheng et al., 2009, 2012a). This phase lag could be attributed to the influence of millennial-scale abrupt climate change in NH high latitudes (Porter and An, 1995; Sun et al., 2012), which delayed the response of ASM to the rising NHSI (Ziegler et al., 2010; Cheng et al., 2012a).

4 Conclusions

In this study, our new spliced δ^{18}O record of five stalagmites from Yangkou cave, Chongqing, exhibits ASM variability over the time period during 124–206 kyr BP. The prominent consistency between the Yangkou and previous Chinese cave δ^{18}O sequences confirms the duration and intensity of the encompassed ASM events in the entire mainland. Our data supports the hypothesis that the ASM change primarily follows NHSI on a precessional timescale. The weakest ASM condition during low-insolation MIS 6.2 was influenced by forcing originating from the North Atlantic. The strongest ASM intensity at MIS 6.5 over the past 500 kyr BP (Cheng et al., 2012b) was presumably partially related to zonal forcing and/or sea level change associated with G–IG dynamics of Walker circulation in the Pacific. More robust geological archives and model simulations are needed to decipher detailed mechanism and forcings for G–IG ASM evolution.

Acknowledgements. We thank J. W. Partin of the Institute for Geophysics, University of Texas-Austin, and G. S. Burr of the Department of Physics, University of Arizona, for their constructive comments. This work was supported by the Taiwan ROC MOST and NTU grants (101-2116-M-002-009, 102-2116-M-002-016 and 101R7625 to CCS). This study was also supported by grants under the National Natural Science Foundation of China (NSFC) (41030103 and 41172165 to TYL, 41072141 and 41272192 to XLY), the Fundamental Research Funds for the Central Universities (XDJK2013A012 to TYL, XDJK2012A003 to XLY), and the Opening fund of the State Key Laboratory of Loess and Quaternary Geology (SKLLQG1310 to TYL).

Edited by: M. Mohtadi

References

Bender, M., Sowers, T., and Labeyrie, L.: The Dole Effect and its variations during the last 130 000 years as measured in the Vostok ice core, Global Biogeochem. Cy., 8, 363–376, 1994.

Cai, Y. J., Cheng, H., An, Z., Edwards, R. L., Wang, X., Tan, L., and Wang, J.: Large variations of oxygen isotopes in precipitation over south-central Tibet during Marine Isotope Stage 5, Geology, 38, 243–246, 2010a.

Cai, Y. J., Tan, L., Cheng, H., An, Z., Edwards, R. L., Kelly, M. J., Kong, X., and Wang, X.: The variation of summer monsoon precipitation in central China since the last deglaciation, Earth Planet. Sc. Lett., 291, 21–31, 2010b.

Cheng, H., Edwards, R. L., Hoff, J., Gallup, C. D., Richards, D. A., and Asmersom, Y.: The half-lives of uranium-234 and thorium-230, Chem. Geol., 169, 17–33, 2000.

Cheng, H., Edwards, R. L., Wang, Y., Kong, X., Ming, Y., Kelly, M. J., Wang, X., Gallup, C. D., and Liu, W.: A penultimate glacial monsoon record from Hulu Cave and two-phase glacial terminations, Geology, 34, 217–220, 2006.

Cheng, H., Edwards, R. L., Broecker, W. S., Denton, G. H., Kong, X., Wang, Y., Zhang, R., and Wang, X.: Ice age terminations, Science, 326, 248–252, 2009.

Cheng, H., Sinha, A., Wang, X., Cruz, F. W., and Edwards, R. L.: The global paleomonsoon as seen through speleothem records from Asia to the Americas, Clim. Dynam., 39, 1045–1062, 2012a.

Cheng, H., Zhang, P., Spötl, C., Edwards, R. L., Cai, Y., Zhang, D., Sang, W., Tan, M., and An, Z.: The climatic cyclicity in semiarid-arid Central Asia over the past 500,000 years, Geophys. Res. Lett., 39, L01705, doi:10.1029/2011GL050202, 2012b.

Cheng, H., Edwards, R. L., Shen, C.-C., Polyak, V. J., Asmerom, Y., Woodhead, J., Hellstrom, J., Wang, Y., Kong, X., and Spötl, C.: Improvements in ^{230}Th dating, ^{230}Th and ^{234}U half-life values, and U-Th isotopic measurements by multi-collector inductively coupled plasma mass spectroscopy, Earth Planet. Sc. Lett., 371–372, 82–91, 2013.

Clemens, S. C., Prell, W. L., and Sun, Y.: Orbital-scale timing and mechanisms driving Late Pleistocene Indo-Asian summer monsoons: reinterpreting cave speleothem δ^{18}O, Paleoceanography, 25, PA4207, doi:10.1029/2010PA001926, 2010.

Clement, A. C., Seager, R., and Cane, M. A.: Orbital controls on the El Niño/Southern Oscillation and the tropical climate, Paleoceanography, 14, 441–456, 1999.

Dayem, K. E., Molnar, P., Battisti, D. S., and Roe, G. H.: Lessons learned from oxygen isotopes in modern precipitation applied to interpretation of speleothem records of paleoclimate from eastern Asia, Earth Planet. Sc. Lett., 295, 219–230, 2010.

DiNezio, P. N. and Tierney, J. E.: The effect of sea level on glacial Indo-Pacific climate, Nat. Geosci., 6, 485–491, 2013.

Dole, M.: The relative atomic weight of oxygen in water and in air a discussion of the atmospheric distribution of the ixygen isotopes and of the chemical standard of atomic weights, J. Chem. Phys., 4, 268–275, 1936.

Hendy, C. H.: The isotopic geochemistry of speleothems – I. The calculation of the effects of different modes of formation on the isotopic composition of speleothems and their applicability as palaeoclimatic indicators, Geochim. Cosmochim. Ac., 35, 801–824, 1971.

Jiang, X., He, Y., Shen, C.-C., Kong, X., Guo, Y., Li, Z., and Chang, Y.-W.: Stalagmite-inferred Holocene precipitation in northern Guizhou Province, China, and asynchronous termination of the climatic optimum in the Asian monsoon territory, Chinese Sci. Bull., 57, 73–79, 2012.

Kelly, M. J., Edwards, R. L., Cheng, H., Yuan D., Cai, Y., Zhang M., Lin, Y., and An, Z.: High resolution characterization of the Asian Monsoon between 146,000 and 99,000 years B.P. from Dongge Cave, China and global correlation of events surrounding Termination II, Palaeogeogr. Palaeocl., 236, 20–38, 2006.

Koutavas, A., Lynch-Stieglitz, J., Marchitto, T. M., and Sachs, J. P.: El Niño-like pattern in ice age tropical Pacific sea surface temperature, Science, 297, 226–230, 2002.

Lachniet, M. S.: Climatic and environmental controls on speleothem oxygen-isotope values, Quaternary Sci. Rev., 28, 412–432, 2009.

Lea, D. W., Pak, D. K., and Spero, H. J.: Climate impact of Late Quaternary Equatorial Pacific sea surface temperature variations, Science, 289, 1719–1724, 2000.

Li, T.-Y., Shen, C.-C., Li, H.-C., Li, J.-Y., Chiang, H.-W., Song, S.-R., Yuan, D.-X., Lin, C. D.-J., Gao, P., Zhou, L. P., Wang, J.-L., Ye, M.-Y., Tang, L.-L., and Xie, S.-Y.: Oxygen and carbon isotopic systematics of aragonite speleothems and water in Furong Cave, Chongqing, China, Geochim. Cosmochim. Ac., 75, 4140–4156, 2011.

Lisiecki, L. E. and Raymo, M. E.: A. Pliocene–Pleistocene stack of 57 globally distributed benthic δ^{18}O records, Paleoceanography, 20, PA1003, doi:10.1029/2004PA001071, 2005.

Maher, B. A. and Thompson, R.: Oxygen isotopes from Chinese caves: records not of monsoon rainfall but of circulation regime, J. Quaternary Sci., 27, 615–624, 2012.

Masson, V., Braconnot, P., Cheddadi, R., Jouzel, J., Marchal, O., and de Noblet, N.: Simulation of intense monsoons under glacial conditions, Geophys. Res. Lett., 27, 1747–1750, 2000.

Oppo, D. W., Rosenthal, Y., and Linsley, B. K.: 2000-year-long temperature and hydrology reconstructions from the Indo-Pacific warm pool, Nature, 460, 1113–1116, 2009.

Pausata, F. S. R., Battisti, D. S., Nisancioglu, K. H., and Bitz, C. M.: Chinese stalagmite δ^{18}O controlled by changes in the Indian monsoon during a simulated Heinrich event, Nat. Geosci., 4, 474–480, 2011.

Petit, J. R., Jouzel, J., Raynaud, D., Barkov, N. I., Barnola, J.-M., Basile, I., Bender, M., Chappellaz, J., Davis, M., Delaygue, G., Delmotte, M., Kotlyakov, V. M., Legrand, M., Lipenkov, V. Y., Lorius, G., Pépin, L., Ritz, C., Saltzman, E., and Stievenard, M.: Climate and atmospheric history of the past 420,000 years from the Vostok ice core, Antarctica, Nature, 399, 429–436, 1999.

Porter, S. C. and An, Z. S.: Correlation between climate events in the North Atlantic and China during the last glaciation, Nature, 375, 305–208, 1995.

Rousseau, D.-D., Wu, N., Pei, Y., and Li, F.: Three exceptionally strong East-Asian summer monsoon events during glacial times in the past 470 kyr, Clim. Past, 5, 157–169, doi:10.5194/cp-5-157-2009, 2009.

Shen, C.-C., Edwards, R. L., Cheng, H., Dorale, J. A., Thomas, R. B., Moran, S. B., Weinstein, S. E., and Hirschmann, M.: Uranium and thorium isotopic and concentration measurements by magnetic sector inductively coupled plasma mass spectrometry, Chem. Geol., 185, 165–178, 2002.

Shen, C.-C., Cheng, H., Edwards, R. L., Moran, S. B., Edmonds, H. N., Hoff, J. A., and Thomas, R. B.: Measurement of attogram quantities of ^{231}Pa in dissolved and particulate fractions of seawater by isotope dilution thermal ionization mass spectroscopy, Anal. Chem., 75, 1075–1079, 2003.

Shen, C.-C., Li, K.-S., Sieh, K., Natawidjaja, D., Cheng, H., Wang, X., Edwards, R. L., Lam, D. D., Hsieh, Y.-T., Fan, T.-Y., Meltzner, A. J., Taylor, F. W., Quinn, T. M., Chiang, H.-W., and Kilbourne, K. H.: Variation of initial ^{230}Th/^{232}Th and limits of high precision U-Th dating of shallow-water corals, Geochim. Cosmochim. Ac., 72, 4201–4223, 2008.

Shen, C.-C., Wu, C.-C., Cheng, H., Edwards, R. L., Hsieh, Y.-T., Gallet, S., Chang, C.-C., Li, T.-Y., Lam, D.-D., Kano, A., Hori, M., and Spötl, C.: U-Th isotopic determinations in femtogram quantities and high-precision and high-resolution carbonate ^{230}Th dating by MC-ICP-MS with SEM protocols, Geochim. Cosmochim. Ac., 99, 71–86, 2012.

Sowers, T., Bender, M., Raynaud, D., Korotkevich, Y. S., and Orchardo, J.: The δ^{18}O of atmospheric O_2 from air inclusions in the Vostok ice core: timing of CO_2 and ice volume changes during the penultimate deglaciation, Paleoceanography, 6, 679–696, 1991.

Sun, X., Li, X., Luo, Y., and Chen, X.: The vegetation and climate at the last glaciation on the emerged continental shelf of the South China Sea, Palaeogeogr. Palaeocl., 160, 301–316, 2000.

Sun, Y., Clemens, S. C., Morrill, C., Lin, X., Wang, X., and An, Z.: Influence of Atlantic meridional overturning circulation on the East Asian winter monsoon, Nat. Geosci., 5, 46–49, 2012.

Tan, L., Cai, Y., An, Z., Edwards, R. L., Cheng, H., Shen, C.-C., and Zhang, H.: Centennial- to decadal-scale monsoon precipitation variability in the semi-humid region, Northern China during the last 1860 years: records from stalagmites in Huangye Cave, Holocene, 21, 287–296, 2011.

Tan, M.: Circulation effect: response of precipitation δ^{18}O to the ENSO cycle in monsoon regions of China, Clim. Dynam., 42, 1067–1077, doi:10.1007/s00382-013-1732-x, 2014.

Taylor, S. R. and McLennan, S. M.: The geochemical evolution of the continental crust, Rev. Geophys., 33, 241–265, 1995.

Wang, B. and Lin, H.: Rainy season of the Asian-Pacific summer monsoon, J. Climate, 15, 386–396, 2002.

Wang, B., Clemens, S. C., and Liu P.: Contrasting the Indian and East Asian monsoons: implications on geologic timescales, Mar. Geol., 201, 5–21, 2003.

Wang, Y., Cheng, H., Edwards, R. L., An, Z., Wu, J., Shen, C.-C., and Dorale, J. A.: A high-resolution absolute-dated Late Pleistocene monsoon record from Hulu Cave, China, Science, 294, 2345–2348, 2001.

Wang, Y., Cheng, H., Edwards, R. L., Kong, X., Shao, X., Chen, S., Wu, J., Jiang, X., Wang, X., and An, Z.: Millennial- and orbital-scale changes in the East Asian monsoon over the past 224,000 years, Nature, 451, 1090–1093, 2008.

Xue, J., Zhong, W., and Zhao, Y.: Variations of $\delta^{18}O$ in precipitation in the Zhujiang (Pearl) river delta and its relationship with

ENSO event, Sci. Geogr. Sin., 27, 825–830, 2007 (in Chinese with English abstract).

Zhang, P., Cheng, H., Edwards, R. L., Chen, F., Wang, Y., Yang, X., Liu, J., Tan, M., Wang, X., Liu, J., An, C., Dai, Z., Zhou, J., Zhang, D., Jia, J., Jin, L., and Johnson, K. R.: A test of climate, sun, and culture relationships from an 1810 year Chinese cave record, Science, 322, 940–942, 2008.

Zhang, R., Zhu, X., Han, D., Zhang, Y., and Fang, F.: Preliminary study on karst caves of Mt. Jinfo, Nanchuan, Chongqing, China, Carsologica Sinica, 17, 196–211, 1998 (in Chinese with English abstract).

Ziegler, M., Tuenter, E., and Lourens, L. J.: The precession phase of the boreal summer monsoon as viewed from the eastern Mediterranean (ODP Site 968), Quaternary Sci. Rev., 29, 481–1490, 2010.